

# RSC Advances



This is an *Accepted Manuscript*, which has been through the Royal Society of Chemistry peer review process and has been accepted for publication.

*Accepted Manuscripts* are published online shortly after acceptance, before technical editing, formatting and proof reading. Using this free service, authors can make their results available to the community, in citable form, before we publish the edited article. This *Accepted Manuscript* will be replaced by the edited, formatted and paginated article as soon as this is available.

You can find more information about *Accepted Manuscripts* in the [Information for Authors](#).

Please note that technical editing may introduce minor changes to the text and/or graphics, which may alter content. The journal's standard [Terms & Conditions](#) and the [Ethical guidelines](#) still apply. In no event shall the Royal Society of Chemistry be held responsible for any errors or omissions in this *Accepted Manuscript* or any consequences arising from the use of any information it contains.

Cite this: DOI: 10.1039/c0xx00000x

www.rsc.org/xxxxxx

ARTICLE TYPE

# Na-X Zeolite Templated and Sulfur-impregnated Porous Carbon as Cathode for High-performance Li-S Battery

Yanhui Cui<sup>1</sup>, Jun Chen<sup>1</sup>, Kevin Huang<sup>2</sup>, Chenqiang Du<sup>3</sup>, Junwei Wu<sup>1\*</sup>, Andrew P. Baker<sup>1</sup>, Xinhe Zhang<sup>4</sup><sup>5</sup> Received (in XXX, XXX) Xth XXXXXXXXX 20XX, Accepted Xth XXXXXXXXX 20XX

DOI: 10.1039/b000000x

Significant efforts have recently been devoted to developing commercially viable high-capacity and low-cost lithium sulfur (Li-S) batteries. In this paper, we report Na-X zeolite templated porous carbon (ZPC) filled with sulfur as a cathode material for Li-S batteries. To immobilize liquid Li sulfide, the surface of NCP was modified by amphiphilic N-polyvinylpyrrolidone (PVP), making ZPC amphiphilic (denoted as A-ZPC). ZPC, A-ZPC and their corresponding composites with sulfur (ZPC-S and A-ZPC-S) were analyzed by various physical characterizations, charge-discharge profiling and electrochemical impedance spectroscopy (EIS). The results showed excellent performance of the A-ZPC-S composite cathode with 46 wt% sulfur loading, a specific capacity can be retained at 691 mAh g<sup>-1</sup> even after 300 cycles under a rate of 1 C, fading only 0.142 % per cycle.

## Introduction

The development of high-capacity energy storage systems is highly desirable for portable electronic devices, power tools, and electric vehicles [1–6]. Li-S batteries have attracted much attention recently as a potential candidate to replace state-of-art Li-ion batteries for high-capacity energy systems such as electric vehicles (EVs). The sulfur cathode in Li-S batteries has a theoretical capacity of 1672 mAh g<sup>-1</sup> and energy density of 2600 Wh kg<sup>-1</sup>, which is nearly 5x a lithium ion battery cathode [7–10]. However, significant challenges remain for the commercialization of Li-S batteries [11–18], including intrinsically low conductivity of elemental sulfur, structural and morphological changes of sulfur during the charge-discharge process, formation of insoluble sulfides Li<sub>2</sub>S<sub>2</sub>/Li<sub>2</sub>S on the Li anode, and the “shuttle effect” that substantially increases the self-discharge [19–20]. The root cause of these problems could be traced to the formation of soluble polysulfide ions during the electrochemical operations. Some strategies have been developed to alleviate the problem, including using separators to restrain lithium sulfides from shuttling between cathode and anode [21–23], covering lithium anode with graphite and V<sub>2</sub>O<sub>5</sub> to limit lithium sulfide formation [24, 25], restricting sulfur within a conductive porous matrix [26–28]. The last one receives special attention due to its simplicity and effectiveness. Thus, main efforts to improve the performances of Li-S batteries have been placed on developing carbon-based sulfur composites, such as carbon spheres with micropores [26], spherical ordered mesoporous carbon with a large number of inner pores [27], porous hollow carbon [28], graphene oxide [29, 30], graphene

[31], porous carbon nanofibers and hollow carbon nanofibers or nanotubes [32–34]. However, applications of these carbon materials are limited because of the complicated preparation process and high cost. Recently, porous hollow carbon spheres were prepared using SiO<sub>2</sub> particles (~100 nm) as a template by the hydrolysis of Tetraethyl orthosilicate (TEOS). The Li-S battery using such carbon spheres exhibited a good cycling performance [35].

In this study, we report Na-X zeolite templated ZPC as a holder of elemental sulfur to serve as a cathode. Since the particles size of zeolite was 30–50 nm, substantially smaller than 100 nm of previously reported [35], it would result in finer carbon particles with larger surface areas, better sulfur-carbon contact and polysulfides retention within the carbon matrix. To improve sulfur retention and thus the cycle life [36], the surface of ZPC was also modified by amphiphilic N-polyvinylpyrrolidone (PVP).

## Experimental

### Preparation of Na-X zeolite, ZPC and A-ZPC

The Na-X zeolite used in this study was synthesized by hydrothermal method [37–39]. First, 6.757 g NaOH was dissolved in 49 g deionized (DI) water and added 3.538 g Al(OH)<sub>3</sub>, then heated at 100 °C to form a transparent solution. After cooled down to room temperature, the solution was stirred in an ice-water bath for 1 h, followed by adding 15 g TEOS and stirring for 6 h. The solution was then cooled down to room temperature and continued to stir for another 24 h. The conditions for hydrothermal crystallization were 60 °C for 2 days. The products were centrifuged and washed with deionized (DI) water until pH

< 10, and finally dried at 80 °C for 24 h.

The ZPC was fabricated using the synthesized Na-X zeolite as a template. First, 4.5 g Na-X zeolite was immersed in 60 ml ethanol with sonication for 1 h. Meanwhile 2.0 g phenolic resin was dissolved in 80 ml ethanol at 50 °C. Then these two solutions were mixed and stirred for 15 min. After that, a mixture of 40 mL of the concentrated aqueous ammonia and 100 mL of ethanol was quickly added to the solution and stirred for 3 h. The obtained slurry was then evaporated for 12 h at 60 °C and the dried solid was fired for 2 h at 850 °C under nitrogen gas flow in a tubular furnace. The obtained black solid was subsequently washed with 1M HCl and 10 wt% HF solution to remove the aluminum and silica, respectively, followed by repeated centrifuging with distilled water until the pH reached ~7. The black product was finally dried at 80 °C to be ZPC.

The A-ZPC preparation was some difference from that of ZPC. Before washed with HCl and HF, the product was immersed and sonicated 5 min in 5 wt% PVP (M.W. = 55000) solution of methanol. Subsequently, the product was filtrated and washed with DI water. Then the following steps were same as ZPC preparation.

#### Preparation of ZPC-S and A-ZPC-S composite

The carbon-sulfur composites were fabricated via a melt-diffusion method. The ZPC (A-ZPC) and sulfur were first intimately mixed and then heated to 155 °C in a sealed vessel under an argon atmosphere with a heating rate of 5 °C min<sup>-1</sup>. After 10 h, a carbon-sulfur composite was obtained.

#### Characterizations

The morphology was examined by scanning electron microscopy (SEM) (Hitachi S4700), coupled with a probe for energy-dispersive scanning (EDS). A thin Au layer was coated on the surface of ZPC to prevent charging.

The external and specific surface areas of the samples were obtained from N<sub>2</sub> adsorption isotherms measured with a Belsorp-max (Japan). The ZPC and A-ZPC were preheated above 100 °C for 3 h at 0.1 kPa prior to measurement.

Fourier transform infrared spectra (FT-IR) were collected on a NICOLET-380, to get more information of ZPC (A-ZPC). Infrared spectra were collected from the average of 32 scans with a resolution 2 cm<sup>-1</sup> over the range 4000–400 cm<sup>-1</sup>.

The binding energy of sulfur in composite materials was further analyzed by X-ray photoelectron spectroscopy (XPS) with a Kratos AXIS Ultra DLD.

The weight ratio of sulfur in the ZPC-S and A-ZPC-S composite was quantified by a NETZSCH STA 449F3 thermal analyzer in N<sub>2</sub> atmosphere at a heating rate of 10 °C min<sup>-1</sup>. The sulfur content in a ZPC-S composite was the mass loss of ZPC-S at 450 °C. But the sulfur content in a A-ZPC-S composite was calculated by the mass loss of A-ZPC-S at 450 °C:  $M_L = x + (1-x) \times 16.4\%$ , where  $x$  is the sulfur content in A-ZPC-S composite; 16.4% is the mass loss of A-ZPC at 450 °C;  $M_L$  is the mass loss of A-ZPC-S at 450 °C.

#### Electrochemical measurements

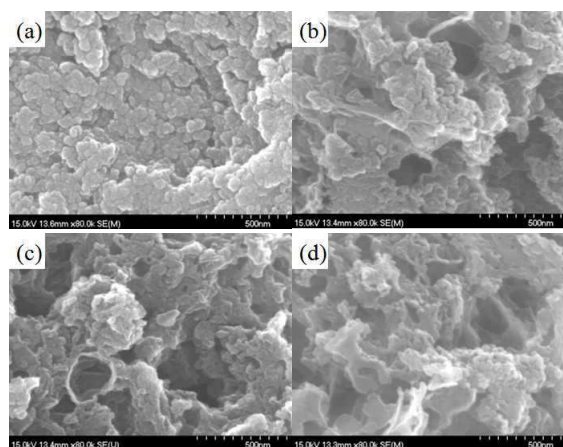
Electrochemical evaluations were performed on CR2032 coin type cells. The cathodes were prepared from a mixture of the ZPC-S (or A-ZPC-S) composites, carbon black (super P), and

Polyvinylidene Fluoride (PVDF) in N-methyl-2-pyrrolidone, with a weight ratio of 80:10:10. The obtained slurry was first uniformly pasted onto an aluminum foil, and dried at 50 °C for 24 h. Lithium metal was used as the anode as well as reference electrode. The electrolyte was a mixture of 1.0 M lithium bis(trifluoromethanesulfonyl)imide (LiTFSI) and 0.1M LiNO<sub>3</sub> dissolved in 1,3-dioxolane (DOL) and 1,2-dimethoxyethane (DME) (1:1, v/v). The coin cells were assembled in an argon-protected glove box (Mikrouna Universal 2440/750). Galvanostatic charge-discharge profiling was performed in a voltage window of 1.7–2.6 V at different rates using a LAND-CT2001A battery testing instrument. The electrochemical performance was also analyzed by electrochemical impedance spectrum (EIS) within a frequency range of 100000 to 0.01 Hz before discharge. The measurements were all conducted at room temperature.

## Results and discussion

### Morphologies of prepared template and electrodes

The morphologies of Na-X zeolite, ZPC, A-ZPC and A-ZPC-S are shown in Fig. 1. As is seen in Fig. 1 (a), the Na-X zeolite is nano-sized, consisting of 30-40 nm sphere particles and apt to agglomerate. Fig. 1(b) shows the SEM image of the ZPC, where the pores created by HCl/HF leaching of zeolite are visible (The Na-X content in ZPC analyzed by EDS is given in Fig. S2). The pore sizes displayed are larger than zeolite particle size because the nano-sized zeolite particles are agglomerated easily and difficult to disperse completely. Similarly, the morphology and pore size of A-ZPC is close to that exhibited by ZPC, as shown in Fig. 1 (c). TEM images (Fig. 1(e) and (f)) show that A-ZPC has a better dispersion than ZPC. This can be ascribed to the amphiphilic nature of PVP (see Fig. S4 for evidence of PVP indicated by FTIR). Fig. 1(d) shows the SEM morphology of A-ZPC filled with 46 wt% sulfur (TGA results are shown in Fig. S3). Additional TEM examination of Fig. 1(g) shows agglomerated particles after sulphur loadings. Furthermore, from EDS mapping, it is clearly shown that sulfur distributes uniformly in A-ZPC (see Fig. S6).



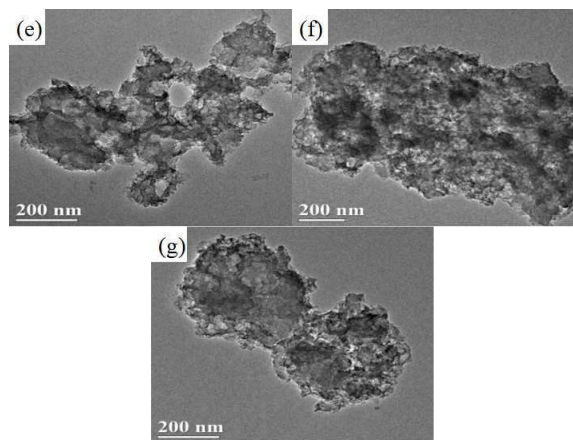


Fig. 1 The SEM images of (a) Na-X zeolite, (b) ZPC, (c) A-ZPC and (d) A-ZPC-S composite with 46 wt% sulfur; TEM images of (e) ZPC, (f) A-ZPC and (g) A-ZPC-S composite with 46 wt% sulfur

### Surface areas of Na-X zeolite, ZPC, A-ZPC and A-ZPC/S

Fig. 2(a) and 2(b) show the  $N_2$  adsorption and desorption isotherms and pore size distributions, respectively, of Na-X zeolite, ZPC, A-ZPC and A-ZPC-S. Type I isotherm of the Na-X zeolite reveals it as a typical microporous material. The isotherms of all other materials fell into the category of Type IV, suggesting them as meso-porous materials [40, 41]. Both surface area and pore volume of A-ZPC are larger than that of ZPC because of the PVP dispersant, leading to a better dispersion of A-ZPC. Fig. 2(b) shows a comparison of pore distributions of ZPC, A-ZPC and A-ZPC loaded with 46 wt% sulfur. It is evident that the majority of pore sizes are less than 10 nm for both ZPC and A-ZPC. Once sulfur was impregnated, the pores were occupied and the surface area was decreased dramatically. The values obtained from the isotherms are tabulated in Table S1.

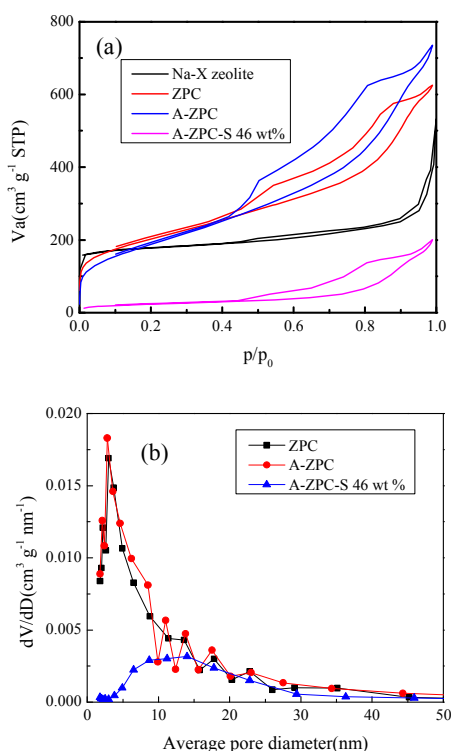


Fig. 2 (a) The  $N_2$  adsorption and desorption curves and (b) pores distribution of Na-X zeolite, ZPC, A-ZPC and A-ZPC-S 46 wt% sulfur composite

### Electrochemical performances

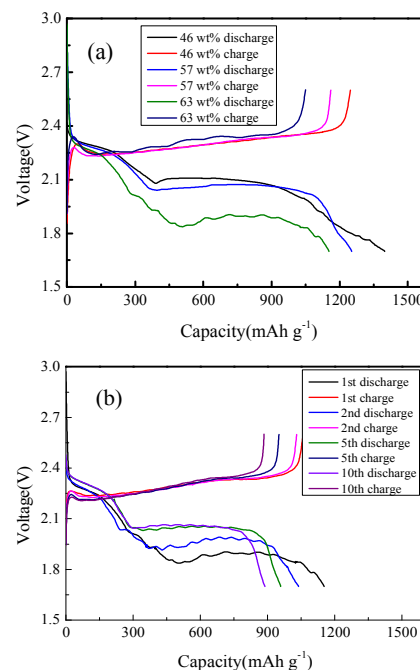


Fig. 3 (a) The first discharge/charge curves of the A-ZPC-S composites with different sulfur contents at 0.2C rate at a voltage window of 1.7-2.6V and (b) the charge/discharge curves of the A-ZPC-S composites with 63 wt% sulfur

Fig. 3 (a) shows the initial discharge and recharge curves at 0.2 C for the A-ZPC electrodes with various loadings of sulfur (The current at 1 C is equivalent to 1672 mAh  $g^{-1}$ ). A typical 2-stage discharge curve related to sulfur reduction was observed for all electrodes. The discharge plateaus started to decrease and become rough as the sulfur loading reaches as high as 63 wt%. From Fig. 3 (b), it is noted that the voltage of the second plateau recovered after several cycles at the sacrifice of capacity loss. The potential recovery may result from the dissolution and re-deposition of soluble polysulfide, which can improve the sulfur distribution in the carbon matrix. In addition, the recovery also suggests an activation process in the initial several cycles, because the deeply buried sulfur and disulfide bonds can only gradually contact with the electrolyte and become electrochemically active [42]. It is also noted that the discharge curves become smoother with cycles. It could be explained that every time as the fresh sulfur becomes electrochemically active, there will be a supersaturation point, a “knee”, of discharge voltage [8], thus the discharge curves show ups and downs curves in the initial several cycles. After the entire loaded sulfur becomes electrochemically active, the discharge curves show smooth again. It is noted from Fig. 3(a) that the lower the surface area, the less the discharge capacity. The initial discharge capacities are 1398, 1253 and 1152 mAh  $g^{-1}$  for the composite with 46%, 57% and 63 wt% sulfur, respectively, while the corresponding initial charge capacity are 1246, 1160 and 1049 mAh  $g^{-1}$  with coulombic efficiencies of 89.1%, 92.6% and 91.9% respectively. The largest irreversible capacity occurred in first

RSC Advances Accepted Manuscript

cycle is due to the polarization of electrode and irreversible capacity of carbon as indicated by Fig. S1.

The cycle performances of ZPC and A-ZPC electrodes with various sulfur loadings are shown in Fig. 4. All batteries were discharged at 0.5C between a voltage window of 2.6-1.7 V. Fig. 4(a) shows the same trend for ZPC-S composite electrodes. The first discharge capacities of the composite with 44 wt%, 52 wt% and 60 wt% sulfur are 1035, 1028, 973 mAh g<sup>-1</sup> respectively, whereas they are 701, 715, 676 mAh g<sup>-1</sup> after the 50th discharge capacities, indicating a degradation rate of 32.3%, 30.4% and 30.5%, respectively. It is noted that the lowest capacity is from the composite with 60 wt% sulfur. According to the BET results of the pore volume of 0.954 cm<sup>3</sup> g<sup>-1</sup>, considering the volume change in the process of charge and discharge, the max suitable mass of sulfur loading can be calculated based on Li<sub>2</sub>S content.

$$m_s = V_p \cdot \rho_{Li_2S} \cdot M_s / M_{Li_2S} \quad [1]$$

$V_p$  is the pore volume of per gram carbon,  $\rho_{Li_2S}$  is the density of Li<sub>2</sub>S (1.66g cm<sup>-3</sup>),  $M_s$  and  $M_{Li_2S}$  are molar masses of sulfur (32 g mol<sup>-1</sup>) and Li<sub>2</sub>S (46 g mol<sup>-1</sup>), respectively. So the max suitable mass of sulfur impregnated in the pores per gram of carbon is about 52 wt%. For 60 wt% sulfur loading, the pore volume is not enough for the expansion/extraction during charge and discharge process. Therefore, the lower capacity is attributed to the limited pore volume and contact surface area between sulfur and carbon, which do not increase proportionately with the sulfur loadings, leading to some sulfur unutilized.

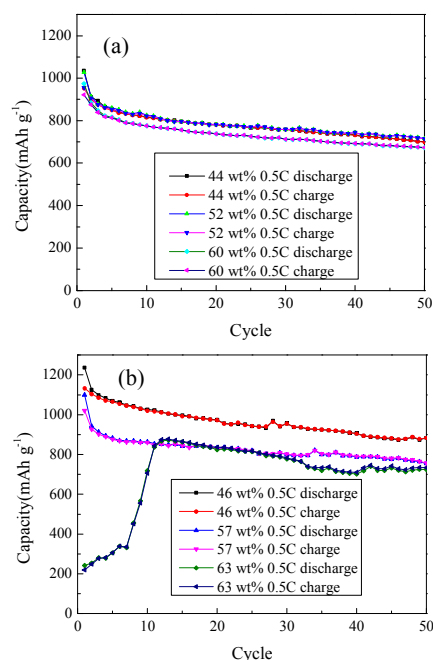


Fig. 4 The cycling performance of (a) ZPC-S and (b) A-ZPC-S composite with different sulfur content at 0.5C between 1.7V and 2.6V

Regardless the sulfur loadings, discharge capacities of the A-ZPC-S composite in Fig. 4 (b) display a higher value than that of ZPC-S composites. This is because the electrode has a higher surface area, more pores and stronger interactions between polar carbon and polar Li<sub>x</sub>S clusters in A-ZPC-S composite [36]. It is also noted that the composite with 63 wt% sulfur loadings

displays a lower initial discharge capacity of 241 mAh g<sup>-1</sup>, followed by a gradual increase to the highest capacity of 877 mAh g<sup>-1</sup> at the 12<sup>th</sup> cycle, suggesting an activation process existed in A-ZPC-S composite electrode. The discharge curves of the activation process are shown in Fig. S7. For the composite with 46 wt% and 57 wt% sulfur loadings, no activation process is observed, indicating the contact surface area is enough for the charge and discharge process. For the composite with lower sulfur loadings, the cycle performance is relatively stable. For example, with 46 wt% sulfur loading, the first discharge and 50th cycle discharge capacities are 1236 and 884 mAh g<sup>-1</sup>, respectively, fading at 28.5% or 0.57% per cycle. For 57 wt% sulfur loading, 1099 mAh g<sup>-1</sup> for the reversible capacity and 754 mAh g<sup>-1</sup> for 50th discharge capacity with a fading rate of 31.4% or 0.63% per cycle. The larger fading rate for 57 wt% sulfur loading is due to the higher sulfur content exceeding the suitable sulfur content in A-ZPC-S (56%, for  $V_p$  as 1.113cm<sup>3</sup> g<sup>-1</sup>). Overall, for low sulfur loading, A-ZPC-S composite behaves better than ZPC-S composite, due to its higher surface area, more pores and a strong interaction between the amphiphilic carbon and polar Li<sub>x</sub>S clusters [36]. The latter is confirmed by XPS shown in Fig. 5, where the S 2p binding energy of A-ZPC-S is shifted by at least 0.1 eV. In particular, the highest binding energy of A-ZPC-S (170.4eV) is 0.9eV larger than that of ZPC-S (169.5eV). The larger binding energy indicates the shuttling phenomenon could be suppressed, leading to a better cycle life [36]. (The sulfur content before cycle and after cycling was shown in Table S2).

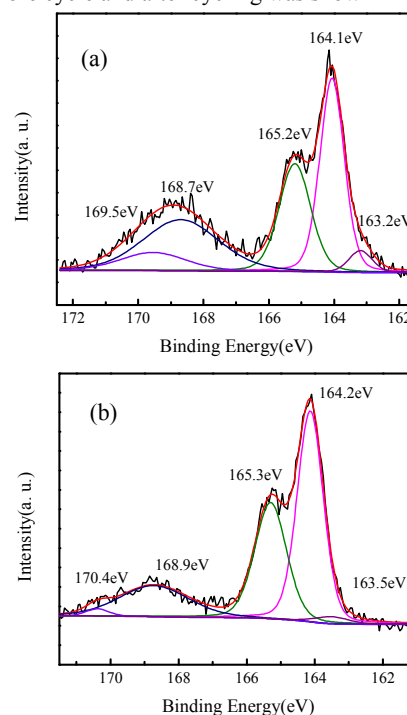


Fig. 5 XPS spectra of S 2p for (a) ZPC-S and (b) A-ZPC-S

In addition, the better electrochemical performance of A-ZPC-S to that of ZPC-S was also confirmed by EIS before discharge; the results are shown in Fig. 6. Each spectrum includes a semicircle in high to medium frequency region and an inclined line in the lowest frequency region. The high to medium frequency semicircle is deemed related to the charge transfer resistance ( $R_{ct}$ ) and the low-frequency sloped line corresponds to

ion diffusion within the cathodes [43]. In equivalent circuit inset in Fig. 6,  $R_e$  is the resistance of electrolyte,  $R_1/CPE_1$  is the resistance of SEI layer and its relative capacitance (Here they equal 0 because SEI layer hasn't formed before cycle),  $R_{ct}/CPE_2$  is the charge transfer resistance and its relative capacitance. For both ZPC-S and A-ZPC-S,  $R_{ct}$  increases with sulfur loading, probably because of sulfur agglomerate causing poor contact with carbon. In addition,  $R_{ct}$  of A-ZPC-S increases faster at higher sulfur content than ZPC-S. This is due to PVP on the surface of A-ZPC that changed the polarity of carbon and led to more agglomeration of sulfur. However, the agglomeration is expected to decrease with the charge and discharge cycle, leading to decreased  $R_{ct}$  as shown in Fig. S5. A little smaller  $R_{ct}$  for A-ZPC-sulfur with 46 wt% sulfur loading than ZPC-S with 44 wt% sulfur loading is probably due to the enough pore volume of the former to infill sulfur, leading to less agglomeration of sulfur on the carbon surface.

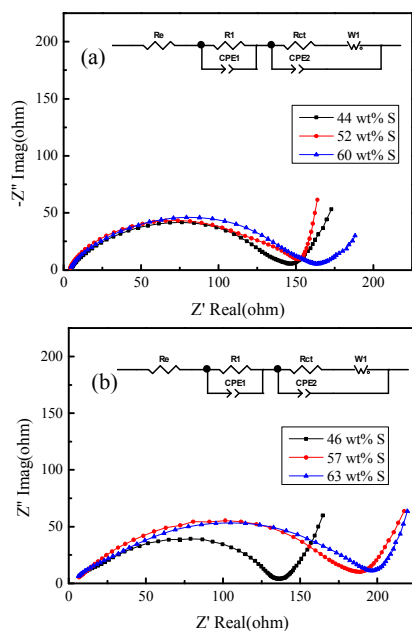


Fig. 6 EIS of as-prepared (a) ZPC-S and (b) A-ZPC-S composite electrodes in Li-S batteries

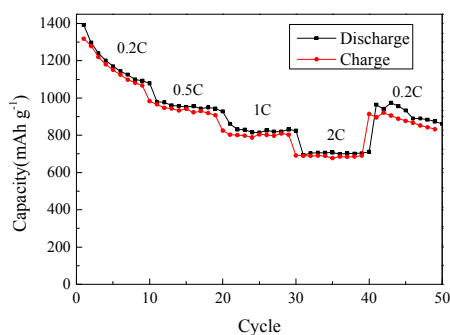


Fig. 7 Rate capability behaviors of A-ZPC composite with 46 wt% sulfur at different current density from 0.2C to 2C between 1.7V and 2.6V

The A-ZPC-S composite with 46 wt% sulfur was shown to possess the best cycle performance and highest capacity at 0.5C rate in Fig. 4. Therefore its rate performance was investigated further. The rate capability behaviors at different current density from 0.2C to 2C between 1.7V and 2.6V are shown in Fig. 7. A reversible capacity of 1391, 979, 861 and 694 mAh g<sup>-1</sup> can be obtained at 0.2, 0.5, 1C and 2 C, respectively, owing to the large surface area of A-ZPC matrix. The capacity of ~ 964 mAh g<sup>-1</sup> can

be retained when the rate is reduced to 0.2 C after 40 cycles, showing a good abuse tolerance of Li-S battery under different current densities.

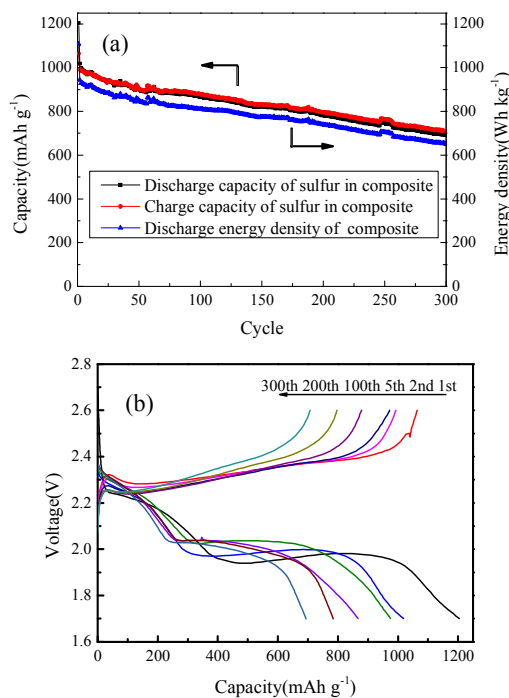


Fig. 8 (a) The cycling performance and (b) the discharge/charge curves of A-ZPC composite with 46 wt% sulfur content at 1C between 1.7V and 2.6V

The long-term cycling performance of the A-ZPC-S composite with 46 wt% sulfur was investigated further at 1C rate between 1.7 and 2.6 V. As shown in Fig. 8(a), the first discharge capacity of 1204 mAh g<sup>-1</sup> can be obtained at 1 C. The reversible capacity retains about 691 mAh g<sup>-1</sup> over 300 cycles, with a high coulombic efficiency of 97.6%. The faded capacity is 513 mAh g<sup>-1</sup>, 42.6 % of the first discharge capacity, with a fading rate of 0.142 % per cycle. From Fig. 8(b), the second discharge plateaus increase at the first five cycles due to  $R_{ct}$  decrease and no obvious decrease after 300 cycles, implying that the A-ZPC-S composites have good stability.

## Conclusions

In summary, nanoporous carbon particles have been successfully prepared by nano-sized Na-X zeolite particles as a template for high-performance Li-S batteries. This method is simple and repeatable. Compared to the ZPC-S composite, the ZPC whose surface was amphiphilically modified by PVP (denoted as A-ZPC) exhibited improved capacity and cycling performance. The A-ZPC-S composite with 46 and 57 wt% sulfur loading showed a discharge capacity of 884 and 754 mAh g<sup>-1</sup>, respectively, after 50 cycles at 0.5C. In particular, the A-ZPC-S (46 wt% sulfur) cathode exhibited a reversible capacity of 691 mAh g<sup>-1</sup> after 300 cycles, fading only 0.142% per cycle. The amphiphilicity of the A-ZPC made the trapping of soluble polysulfide species easier. These results showed that A-ZPC is an excellent placeholder for sulfur and a promising cathode for high-performance Li-S batteries.

RSC Advances Accepted Manuscript

## Acknowledgements

This work is supported by the International Collaboration Program of Shenzhen (GJHZ20150312114008636, GJHZ20130411141529167), Shenzhen Peacock Plan Program (KQCX20140521144358003), Fundamental Research Program of Shenzhen (JCYJ20140417172417144, JCYJ20130329141705731), and the project of Innovative group for high-performance lithium-ion power batteries R&D and industrialization of Guangdong Province (Grant No. 2013N079).

## Notes and references

<sup>1\*</sup> Department of Materials Science and Engineering, Harbin Institute of Technology Shenzhen Graduate School, Shenzhen Key Laboratory of Advanced Materials, Shenzhen 518055, China. Fax: 86-755-2603 3504; Phone: 86-755-2603 3290; [junwei.wu@hitsz.edu.cn](mailto:junwei.wu@hitsz.edu.cn)

<sup>2</sup> Department of Mechanical Engineering, University of South Carolina, Columbia, SC 29201, USA.

<sup>3</sup> Department of Applied Chemistry, Tianjin University, Tianjin 300072, China

<sup>4</sup> Dongguan McNair Technology Co., Ltd, Dongguan City, Guangdong 523700, China

† Electronic Supplementary Information (ESI) available: (S1) charge and discharge curves of the A-ZPC, (S2) EDS of Na-X zeolite and A-ZPC, (S3) TG of ZPC/A-ZPC and ZPC-S/A-ZPC-S, (S4) FTIR of ZPC and A-ZPC, (S5) EIS of A-ZPC-S composite with 63 wt% sulfur loading after different cycles at 0.2C, (S6) SEM image of A-ZPC-S composite with 46 wt% sulfur and EDX element mappings of S and O, (S7) The discharge curves of A-ZPC-S composite with 63 wt% sulfur content at 0.5C between 1.7V and 2.6V, (S8) SEM images of A-ZPC-S composite with 46 wt% sulfur cathode before cycling and the cathode after 300 cycles at 1C, (S9) The cycling performance of ZPC-S 44 wt% sulfur and A-ZPC-S 46 wt% sulfur at 1C, (S10) The EDS of cathode ZPC-S 44 wt% sulfur and A-ZPC-S 46 wt% before cycling and after 300 cycling at 1C, (S11) surface area, pore volume and average pore size of zeolite, ZPC, A-ZPC and A-ZPC-S composite, (S12) The sulfur maintenance of ZPC-S cathode and A-ZPC-S cathode after 300 cycles at 1C. See DOI: 10.1039/b000000x/

‡ Footnotes should appear here. These might include comments relevant to but not central to the matter under discussion, limited experimental and spectral data, and crystallographic data.

- P.G. Bruce, S.A. Freunberger, L.J. Hardwick, J.M. Tarascon, *Nat. Mater.* 11 (2012) 19-29.
- B.L. Ellis, K.T. Lee, L. F. Nazar, *Chem. Mater.* 22 (2010) 691-714.
- E.Hu, S.M. Bak, J. Liu, X. Yu, Y. Zhou, S.N. Ehrlich, K.W. Nam, *Chem. Mater.* 26 (2013) 1108-1118.
- A. Manthiram, Y. Fu, S.H. Chung, C. Zu, Y.S. Su, *Chem. Rev.* 114 (2014) 11751-11787.
- B. Guo, X. Yu, X.G. Sun, M. Chi, Z.A. Qiao, J. Liu, S. Dai, *Energy Environ. Sci.* 7 (2014) 2220-2226.
- Y. Yang, G. Zheng, Y. Cui, *Chem. Soc. Rev.* 42 (2013) 3018-3032.
- A. Manthiram, Y. Fu, Y.S. Su, *Acc. Chem. Res.* 46 (2012) 1125-1134.
- L.F. Nazar, M. Cuisinier, Q. Pang, *MRS Bull.* 39 (2014) 436-442.
- X. Ji, L.F. Nazar, *J. Mater. Chem.* 20 (2010) 9821-9826.
- S. Evers, L.F. Nazar, *Acc. Chem. Res.* 46 (2012) 1135-1143.
- Z. Li, Y. Jiang, L.Yuan, Z. Yi, C. Wu, Y. Liu, S. Peter, Y. Huang, *ACS Nano* 8 (2014) 9295-9303.
- L. Xiao, Y. Cao, J. Xiao, B. Schwenzer, M.H. Engelhard, L.V. Saraf, Z. Nie, G.J. Exarhos, J. Liu, *Adv. Mater.* 24 (2012) 1176-1181.
- S. Zheng, F. Yi, Z. Li, Y. Zhu, Y. Xu, C. Luo, J.H. Yang, C. Wang, *Adv. Funct. Mater.* 24 (2014) 4156-4163.
- C. Zu, A. Manthiram, *Adv. Energy Mater.* 3 (2013) 1008-1012.
- L. Sun, M. Li, Y. Jiang, W. Kong, K. Jiang, J. Wang, S. Fan, *Nano Lett.* 14 (2014) 4044-4049.

- R. Elazari, G. Salitra, A. Garsuch, A. Panchenko, D. Aurbach, *Adv. Mater.* 23 (2011) 5641-5644.
- Z. Feng, C. Kim, A. Vijh, M. Armand, K.H. Bevan, K. Zaghbi, *J. Power Sources* 272 (2014) 518-521.
- R.S. Assary, L.A. Curtiss, J.S. Moore, *J. Phys. Chem. C* 118 (2014) 11545-11558.
- Y.V. Mikhaylik, J.R. Akridge, *J. Electrochem. Soc.* 151 (2004) A1969-A1976.
- S.K. Lee, S.M. Oh, E. Park, B. Scrosati, J. Hassoun, M.S. Park, Y.J. Kim, H. Kim, L. Belharouak, Y.K. Sun, *Nano Lett.* 15 (2015) 2863-2868.
- Y. Chen, N. Liu, H. Shao, W. Wang, M. Gao, C. Li, H. Zhang, A. Wang, Y. Huang, *J. Mater. Chem. A* 3 (2015) 15235-15240.
- J.Q. Huang, Q. Zhang, H.J. Peng, X.Y. Liu, W.Z. Qian, F. Wei, *Energy Environ. Sci.* 7 (2014) 347-353.
- Z. Liu, X.H. Zhang, C.S. Lee, *J. Mater. Chem. A* 2 (2014) 5602-5605.
- C. Huang, J. Xiao, Y. Shao, J. Zheng, W.D. Bennett, D. Lu, S.V. Laxmikant, M. Engelhard, L. Ji, J. Zhang, X. Li, G.L. Graffl, J. Liu, *Nature Comm.* 5 (2014).
- W. Li, J. Hicks-Garner, J. Wang, J. Liu, A.F. Gross, E. Sherman, J. Graetz, J.J. Vajo, P. Liu, *Chem. Mater.* 26 (2014) 3403-3410.
- B. Zhang, X. Qin, G.R. Li, X.P. Gao, *Energy Environ. Sci.* 3 (2010) 1531-1537.
- J. Schuster, G. He, B. Mandlmeier, T. Yim, K.T. Lee, T. Bein, L.F. Nazar, *Angew. Chem., Int. Ed.* 51 (2012) 3591-3595.
- N. Jayaprakash, J. Shen, S.S. Moganty, A. Corona, L.A. Archer, *Angew. Chem., Int. Ed.* 123 (2011) 6026-6030.
- L. Ji, M. Rao, H. Zheng, L. Zhang, Y. Li, W. Duan, J. Guo, E.J. Cairns, Y. Zhang, *J. Am. Chem. Soc.* 133 (2011) 18522-18525.
- N. Li, M. Zheng, H. Lu, Z. Hu, C. Shen, X. Chang, G. Ji, J. Gao, Y. Shi, *Chem. Comm.* 48 (2012) 4106-4108.
- H.Wang, Y. Yang, Y. Liang, J.T. Robinson, Y. Li, A. Jackson, Y. Cui, H. Dai, *Nano Lett.* 11 (2011) 2644-2647.
- L.W. Ji, M.M. Rao, S. Aloni, L. Wang, E.J. Cairns, Y.G. Zhang, *Energy Environ. Sci.* 4 (2011) 5053-5059.
- G. Zheng, Y. Yang, J.J. Cha, S.S. Hong, Y. Cui, *Nano Lett.* 11 (2011) 4462-4467.
- J. Guo, Y. Xu, C. Wang, *Nano Lett.* 11 (2011) 4288-4294.
- K. Zhang, Q. Zhao, Z. Tao, J. Chen, *Nano Res.* 6 (2013) 38-46.
- G. Zheng, Q. Zhang, J.J. Cha, Y. Yang, W. Li, Z.W. She, Y. Cui, *Nano Lett.* 13 (2013) 1265-1270.
- F. Pan, X. Lu, Y. Wang, *Microporous Mesoporous Mater.* 184 (2014) 134-140.
- Y. Cui, A.P. Baker, X. Xu, Y. Xiang, L. Wang, M. Lavorgna, J. Wu, *J. Power Sources* 294 (2015) 369-376.
- B.Z. Zhan, M.A. White, M. Lumsden, *Chem. Mater.* 14 (2002) 3636-3642.
- Y.S. Su, A. Manthiram, *Nat. Commun.* 3 (2012).
- Z. Fan, Y. Liu, J. Yan, G. Ning, Q. Wang, T. Wei, L. Zhi, F. Wei, *Adv. Energy Mater.* 2 (2012) 419-424.
- L. Xiao, Y. Cao, J. Xiao, B. Schwenzer, M.H. Engelhard, L.V. Saraf, Z. Nie, G.J. Exarhos, J. Liu, *Adv. Mater.* 24 (2012) 1176-1181.
- L. Yin, J. Wang, F. Lin, J. Yang, Y. Nuli, *Energy Environ. Sci.* 5 (2012) 6966-6972.

